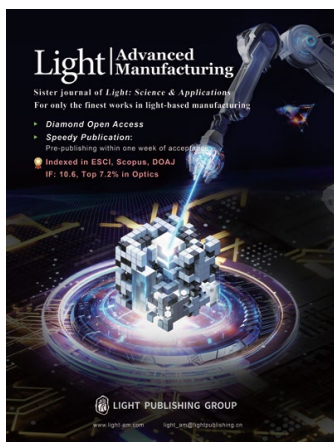


Accepted Article Preview: Published ahead of advance online publication



## Dielectrophoretic-Assisted Trapped-Assembly for Fin-LED Display

Minji Ko, Yuna Kwon, SeungJe Lee, Heemin Oh, Keyong Nam Lee, Young Rag Do

Cite this article as: Minji Ko, Yuna Kwon, SeungJe Lee, Heemin Oh, Keyong Nam Lee, Young Rag Do. Dielectrophoretic-Assisted Trapped-Assembly for Fin-LED Display. *Light: Advanced Manufacturing* accepted article preview 16 January, 2026; doi: 10.37188/lam.2026.026

This is a PDF file of an unedited peer-reviewed manuscript that has been accepted for publication. LAM are providing this early version of the manuscript as a service to our customers. The manuscript will undergo copyediting, typesetting and a proof review before it is published in its final form. Please note that during the production process errors may be discovered which could affect the content, and all legal disclaimers apply.

Received 30 August 2025; revised 15 January 2026; accepted 16 January 2026;  
Accepted article preview online 16 January 2026

1 **Dielectrophoretic-Assisted Trapped-Assembly for**  
2 **Fin-LED Display**

3 **Minji Ko<sup>1†</sup>, Yuna Kwon<sup>1†</sup>, SeungJe Lee<sup>1</sup>, Heemin Oh<sup>1</sup>, Keyong Nam Lee<sup>1</sup> and Young**  
4 **Rag Do<sup>1\*</sup>**

5 <sup>1</sup> Department of Chemistry, Kookmin University, Seoul 02707, Republic of Korea

6 [\\*yrdo@kookmin.ac.kr](mailto:yrdo@kookmin.ac.kr)

7

8

9

10

11

12

13

14

15

16

17

18

19

20

21

22

23

## 1 Abstract

2 We propose a high-precision assembly technique for realizing high-resolution nano- to  
3 microscale displays using a trapped-assembly approach that integrates a doctor-blade-based  
4 ink-delivery system with dielectrophoresis (DEP)-induced assembly. Octadecyltrichlorosilane  
5 (OTS) self-assembled monolayers (SAMs) were coated onto the pixel-defined layer (PDL) to  
6 promote ink trapping and confine fin-LEDs within individual pixels during assembly. Key  
7 process parameters—including the viscosity and dielectric properties of the ink solvent, speed  
8 and number of blade passes, blade-to-substrate gap, and applied DEP voltage and frequency—  
9 were systematically optimised, as these parameters affect solvent confinement of the solvent  
10 and fin-LED assembly behavior. Under optimised conditions, achieved through precise control  
11 of solvent polarity, DEP force and torque, and doctor-blading parameters, all 400 pixels were  
12 successfully assembled. Statistical analysis revealed that 90% of the pixels contained 12-20  
13 fin-LEDs, with an average of 16.3 fin-LEDs per pixel and a standard deviation of 3.5. The  
14 overlap ratio was limited to 8%, and 92% of the fin-LEDs were accurately assembled, of which  
15 95% established contact with the p-GaN surface. Electroluminescent devices fabricated using  
16 the assembled fin-LEDs exhibited bright and uniform emission across the entire pixel array,  
17 confirming their excellent assembly quality and high electrical reliability. The DEP-based  
18 trapped-assembly method provides a reliable and scalable strategy for the practical integration  
19 of nano- to microscale LEDs in next-generation high-resolution display technologies.

20 **Keywords:** GaN, Fin-LED, Trapped-assembly, Dielectrophoresis, Display

21

22

23

24

25

26

27

28

## 1 Introduction

2 Micro-light-emitting diode (micro-LED) displays are emerging as a leading technology for next-  
3 generation display platforms, particularly in augmented reality (AR) and virtual reality (VR)  
4 applications, owing to their remarkably efficient optical performance, extended operational durability,  
5 expansive colour-rendering capability, and robust environmental reliability<sup>1-11</sup>. Positioned to succeed  
6 in OLEDs and conventional LCDs, micro-LEDs are expected to advance both compact and  
7 large-format display applications<sup>12-14</sup>. Recent developments in the micro-LED field have  
8 emphasised not only the importance of achieving full-colour capability but also the stringent  
9 performance requirements associated with next-generation near-eye display applications such as AR  
10 and VR. To simultaneously achieve high colour purity and device miniaturisation, various full-colour  
11 strategies have been actively explored, including RGB monolithic growth, colour-conversion layers  
12 based on quantum dots or perovskite nanocrystals, and heterogeneous RGB transfer processes. Research  
13 in this area has demonstrated that AR and VR systems should achieve high brightness, high external  
14 quantum efficiency, fast response times, and precise pixel alignment to deliver high-resolution displays.  
15 Such demands underscore the need for pixel-level assembly technologies that can provide both high  
16 precision and scalability.<sup>9,10,15</sup> However, their widespread deployment is hindered by critical  
17 technical and economic barriers, including high fabrication costs and the need for highly  
18 scalable and precise pixel-level integration methods<sup>16-20</sup>. Developing a solution to these  
19 challenges is crucial for maximising the potential of micro-LED technologies. Numerous  
20 strategies have been developed for addressing these issues. However, their widespread  
21 adoption is still hindered by critical technical and economic barriers, including high fabrication  
22 costs and the need for highly scalable and precise pixel-level integration methods<sup>16-20</sup>.  
23 Developing a solution to these challenges is crucial for maximizing the potential of micro-LED  
24 technology. Numerous strategies to address these challenges have been investigated. However,  
25 established approaches such as mass transfer<sup>21-26</sup>, laser-assisted transfer<sup>27-31</sup>, and fluidic self-  
26 assembly (FSA)<sup>32-35</sup> still face persistent issues, including misplacement, non-uniform assembly,  
27 and device degradation, particularly for devices smaller than 5  $\mu\text{m}$  in diameter. These  
28 drawbacks are significant obstacles for the integration of micro-LEDs into commercially viable,  
29 high-resolution display systems. To illustrate the structural limitations of these established  
30 approaches more clearly, we provide a quantitative comparison of representative industrial  
31 micro-LED transfer and assembly techniques, including mass-transfer printing, laser-induced  
32 transfer, and fluidic self-assembly (Table 1). This comparison reveals that current

1 methodologies struggle to simultaneously achieve the required alignment precision, throughput,  
 2 and yield for devices with diameters below 5  $\mu\text{m}$ . To overcome these limitations, emerging  
 3 technologies have focused on nano- to microscale inorganic LEDs with dimensions less than 5  
 4  $\mu\text{m}$ <sup>36-40</sup>. As device dimensions shrink, maintaining the desired electro-optical performance  
 5 becomes increasingly critical. Preserving the external quantum efficiency (EQE) while  
 6 simultaneously enabling high-precision assembly and placement is of particular importance.

7  
 8 **Table 1.** Comparison of representative micro-LED transfer and assembly techniques.

Method	Chip size ( $\mu\text{m}$ )	Transfer throughput (units $\text{h}^{-1}$ )	Transfer yield (%)	Alignment precision ( $\mu\text{m}$ )	Cost	Ref.
Mass transfer printing	$\Phi$ : $\sim 5$	$>6.5$ M	99.99%	1.5	Medium	21-26
Laser-induced forward transfer	$\Phi$ : $\sim 50$	$>100$ M	$>90\%$	1.8	High	27-31
Fluidic self-assembly	$\Phi$ : $\sim 50$	$>50$ M	99.88	1.25	Medium	32-35
DEP-assisted trapped-assembly	$3.96 \times 0.72 \times 1.2$	$>1.22$ M	100%	No transfer	Low	Our works

9  
 10 Over the past decade, our research group has developed miniaturised light-emitting diode  
 11 (LED) materials and corresponding integration techniques. By enhancing the integration  
 12 between fluidic deposition strategies and dielectrophoresis (DEP)-assisted assembly, we  
 13 developed a hybrid assembly platform that offers both economic viability and micron-scale  
 14 spatial accuracy<sup>41-46</sup>. In the earlier stages of this research endeavour, we demonstrated the  
 15 integration of nanorod LEDs into displays. However, we noted that nanorods inherently suffer  
 16 from optical leakage owing to edge emission and possess a limited multi-quantum well (MQW)  
 17 volume. To overcome these structural constraints, we adopted an alternative LED structural  
 18 architecture known as fin-LEDs<sup>44</sup>. Fin-LEDs, feature a vertically stacked p-GaN/MQW/n-GaN  
 19 configuration along the short axis, retaining a compact structure comparable to that of nanorods  
 20 while providing a significant optical advantage by concentrating the MQW layers along the  
 21 short axis to enhance forward-directed light extraction. Based on these unique features, fin-  
 22 LEDs are particularly well suited for high-brightness and high-resolution displays. To achieve  
 23 precise directional assembly, we introduced a face-selective DEP technique that improves the  
 24 vertical assembly by inducing torque during DEP. This was accomplished by selectively  
 25 coating low-dielectric materials on the fin-LED sidewalls and integrating an indium tin oxide  
 26 (ITO) layer on the p-GaN surface to influence the rotational behaviour in the applied field.

1 Despite recent advances, the precise placement of nanoscale fin-LEDs on the pixel area  
2 remains a significant challenge. Fluidic-based techniques, such as inkjet printing and  
3 conventional fluidic self-assembly (FSA), suffer from several inherent limitations, including  
4 LED sedimentation, nozzle clogging, and insufficient pixel selectivity<sup>47,48</sup>. These issues  
5 collectively diminish the accuracy and scalability. In recent studies on micro- and nanoscale  
6 assemblies, researchers have extensively explored the use of external forces and capillary-  
7 driven flows to guide the oriented organisation of colloidal nanoscale objects. In this study, a  
8 doctor-blade-based assembly strategy was implemented, in which capillary effects and  
9 dielectrophoretic (DEP) forces were synergistically utilised to uniformly align fin-LEDs within  
10 pixelated regions. Self-assembled monolayers (SAMs) were introduced into the pixel-defining  
11 layers to generate surface-energy contrast, enabling selective confinement of the fin-LED ink  
12 inside each pixel. This localised ink-trapping structure plays a crucial role in enhancing the  
13 directional alignment of fin-LEDs and achieving more uniform placement within individual  
14 pixels.

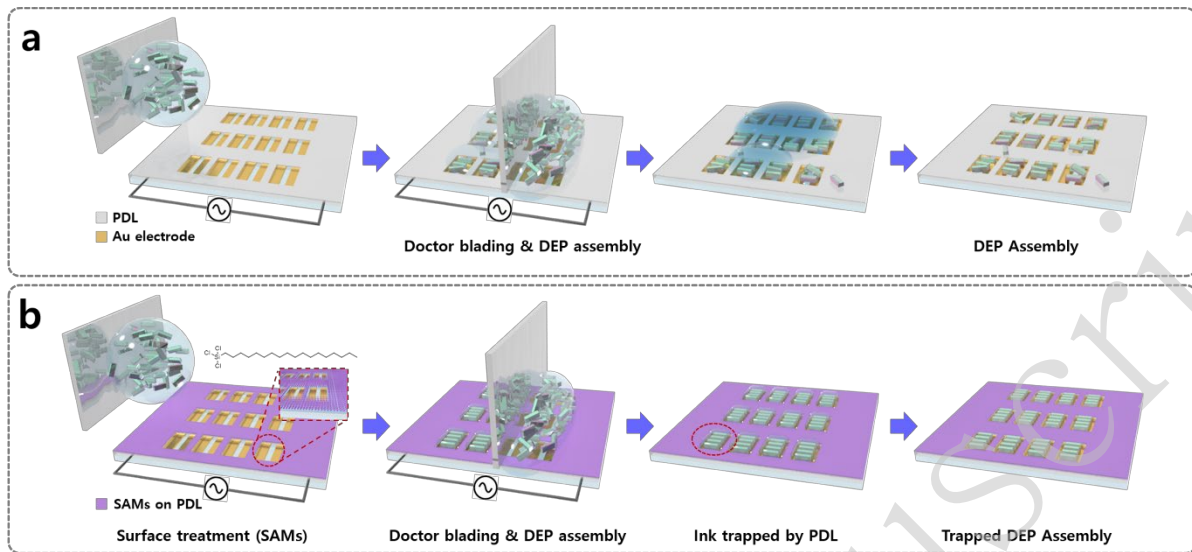
15 To address these technical challenges, we propose a trapped-assembly (TA) method that  
16 combines a doctor-blade-based ink-delivery system with DEP-assisted alignment. This  
17 approach enables the precise and directionally controlled placement of fin-LEDs within  
18 individual subpixels by confining the ink inside pixel-defined regions during assembly. We  
19 systematically optimised key processing parameters, including the viscosity and dielectric  
20 properties of the ink solvent, speed and number of doctor-blade passes, vertical distance  
21 between the blade and the electrodes, and applied DEP voltage and frequency. By precisely  
22 controlling these variables, we effectively confined the ink within each subpixel and achieved  
23 a uniform fin-LED distribution while minimising aggregation and misalignment. Our results  
24 demonstrate that the TA method, which integrates ink confinement with a DEP-based assembly,  
25 enables the highly accurate pixel-level placement of fin-LEDs. This approach provides a  
26 scalable and reliable strategy for fabricating next-generation high-resolution displays with  
27 uniform light emission and reasonable yields.

## 28 29 **Results**

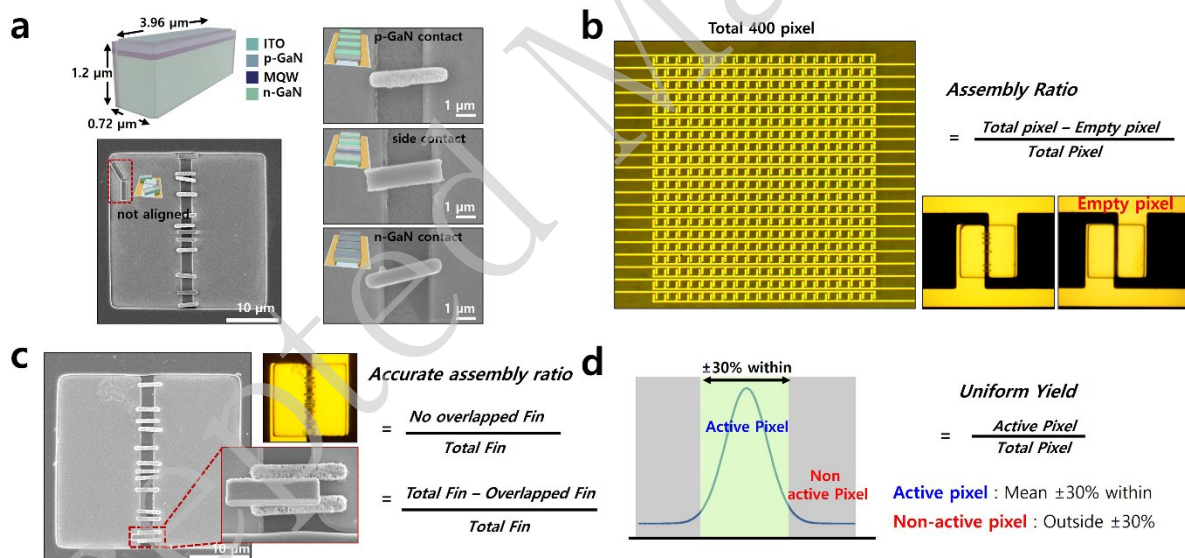
30 The fin-LEDs used in this study were fabricated using the same process as reported in our

1 previous study. A schematic of the fabrication procedure is shown in Fig. S1. The fabricated  
2 fin-LED structures were confirmed using the scanning electron microscopy (SEM) images  
3 shown in Figs. S1f and S1g. Our previous study demonstrated a face-selective assembly  
4 technique for fin-LEDs based on DEP forces. Building on this technology, the present study  
5 introduces a pixel-defined layer (PDL) to enable precise pixel-level assembly and fabricate an  
6 array of 400 pixels. A trapped-assembly approach was implemented by combining doctor-  
7 blade-based ink delivery with DEP-assisted assembly. Fig. 1 presents a schematic of the effects  
8 of PDL surface properties on the trapped-assembly process. Fig. 1a shows the assembly  
9 behaviour without any surface treatment of the PDL. In contrast, Fig. 1b illustrates the trapped-  
10 assembly process, in which the PDL treated with octadecyltrichlorosilane (OTS)-based SAMs  
11 provides a hydrophobic surface that confines the hydrophobic ink within the pixel cavities,  
12 enabling a stable DEP-assisted assembly of the fin-LEDs. Fig. 2 illustrates the evaluation  
13 metrics used to quantitatively assess the accuracy and uniformity of fin-LED assembly Fig. 1.  
14 Fig. 2a shows the SEM images of various contact configurations of the fin-LEDs, depending  
15 on their assembly direction. These include p-GaN contact, n-GaN contact, side contact, and  
16 misassembly. As shown in Fig. 2b, the assembly ratio was calculated by subtracting the number  
17 of empty pixels that contain no fin-LEDs from a total of 400 pixels. Fig. 2c shows the SEM  
18 images used to identify the overlapping fin-LEDs. The assembly ratio was accurately  
19 calculated based on the number of nonoverlapping fins. Fig. 2d illustrates the comparison of  
20 the number of fin-LEDs per pixel with a  $\pm 30\%$  range from the average. Pixels within this range  
21 were defined as ‘Active pixels’, while those outside the range were classified as ‘Non-active  
22 pixels’. This classification enabled the calculation of a uniform yield. During the trapped-  
23 assembly process, the blade was consistently oriented in the direction shown in Fig. S2.

24



1  
2 **Fig. 1.** Schematic of the trapped-assembly process showing the influence of PDL surface properties. **a**  
3 Assembly without PDL surface treatment. **b** Assembly with hydrophobic PDL obtained via OTS-based  
4 SAMs.

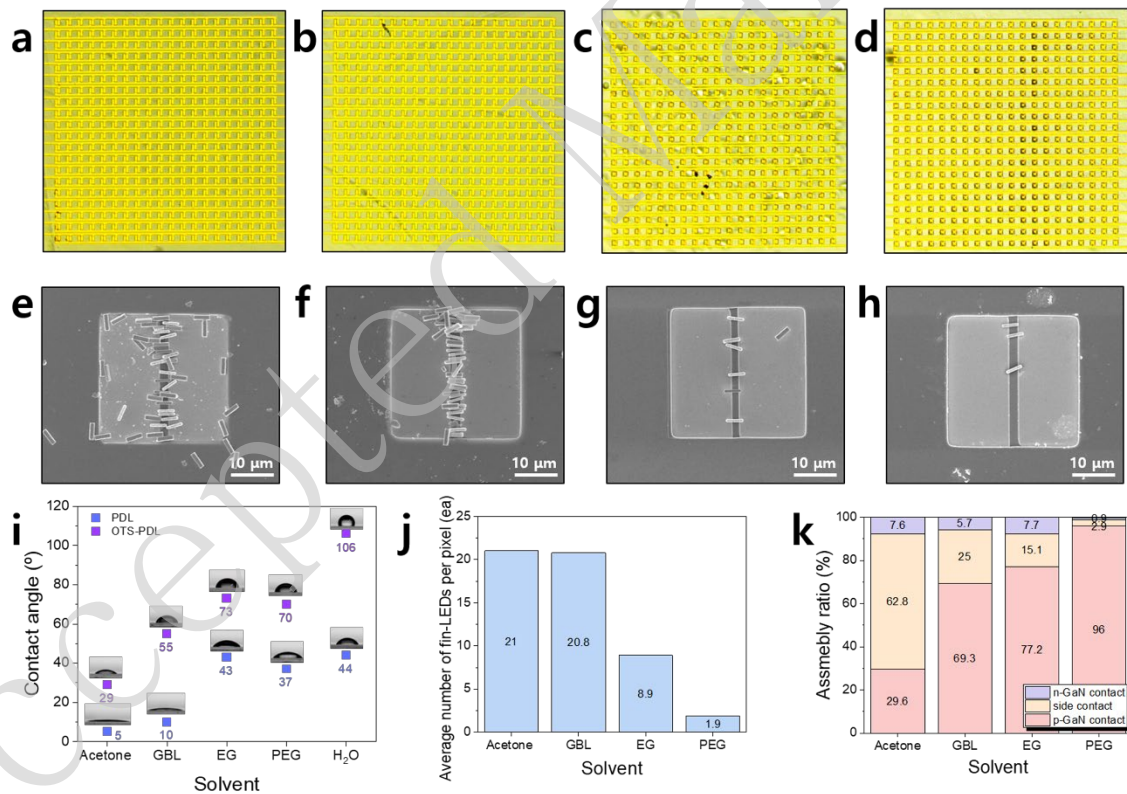


5  
6 **Fig. 2. a** A schematic view of the fin-LED structure with the annotated average dimensions and SEM  
7 images of p-GaN contact, side contact, n-GaN contact, and non-aligned fin-LEDs on the gold electrode.  
8 **b** Definition of assembly ratio based on the number of pixels containing fin-LEDs out of a total of 400  
9 pixels. **c** Definition of accurate assembly ratio and **d** definition of high uniform yield.

10 Fig. S3 shows the assembly results of fin-LEDs on bare PDL without the OTS SAM  
11 treatment using a blade-coating process with different solvents (acetone, gamma-butyrolactone  
12 (GBL), ethylene glycol (EG), and polyethylene glycol (PEG)). As shown in the optical

1 microscopy images (Figs. S3a–S3d), the fin-LED ink was not effectively trapped within the  
2 pixel cavities under any solvent condition. Furthermore, the SEM images (Figs. S3f and S3g)  
3 and assembly ratio calculations (Fig. S3j) revealed that while acetone and GBL exhibited  
4 relatively high p-GaN contact assembly ratios exceeding 80%, the number of fin-LEDs  
5 assembled per pixel was less than 12, and the uniformity of the assembly was notably reduced.  
6 To address this issue, the OTS SAM treatment was introduced to the PDL to facilitate ink  
7 trapping within the pixel cavities, which extended the assembly time and enhanced the  
8 uniformity of the fin-LED assembly. To investigate the interfacial interactions between the fin-  
9 LED ink and the OTS-treated PDL, the assembly behaviour was examined using various  
10 solvents, including acetone, GBL, EG, and PEG. The presence of OTS on the PDL surface was  
11 confirmed by Fourier-transform infrared (FT-IR) spectroscopy. As shown in Fig. S4, the  
12 characteristic C-H stretching peak at 2800–3000  $\text{cm}^{-1}$  indicated the successful formation of the  
13 OTS SAMs. Fig. 3 and Table S1 illustrate the influence of the physical properties of the  
14 solvents and their interfacial interactions with the OTS-treated PDLs on the assembly  
15 behaviour of the fin-LEDs. The four solvents (acetone, GBL, EG, and PEG) exhibited distinct  
16 viscosities, conductivities, dielectric constants, and vapour pressures. Owing to these  
17 differences, the mobility and assembly stability of fin-LEDs varied significantly, even under  
18 identical DEP assembly conditions. The effects of the interfacial interactions between the OTS-  
19 treated PDL and the four solvents with different physical properties (acetone, GBL, EG, and  
20 PEG) on the assembly behaviour of the fin-LEDs are summarised in Fig. 3 and Table S1. These  
21 solvents exhibit notable differences in viscosities, electrical conductivities, dielectric constants,  
22 and vapour pressures. Consequently, even under identical DEP conditions, the mobility and  
23 assembly stability of the fin-LEDs varied significantly depending on the solvent used. In  
24 particular, acetone, which has the lowest viscosity and highest vapour pressure among the  
25 solvents, showed poor solvent trapping within the pixel regions, as observed in the optical  
26 microscopy and SEM images in Fig. 3a and Fig. 3e, respectively. In addition, the SEM image  
27 and data in Fig. 3k revealed that acetone had the lowest p-GaN contact ratio of 29.6%,  
28 indicating poor assembly quality. As shown in the optical microscopy and SEM images in Figs.  
29 3b and 3f, GBL provided an improved fin-LED assembly ratio compared to acetone. In addition,  
30 the p-GaN contact ratio increased to 69.3%, as shown in Fig. 3k. EG, which had a slightly  
31 higher viscosity and lower vapour pressure than GBL, exhibited improved solvent trapping in  
32 the optical microscopy and SEM images in Figs. 3c and 3g, respectively, and the p-GaN contact

1 ratio increased to 77.2%. As shown in the optical microscopy and SEM images in Figs. 3d and  
 2 3h, PEG, the solvent with the highest viscosity and lowest vapour pressure, demonstrated  
 3 effective trapping. It also afforded the highest p-GaN contact ratio of 96%. However, as the  
 4 viscosity increased and the vapour pressure decreased, the number of fin-LEDs assembled per  
 5 pixel decreased significantly, as shown in Fig. 3j. Fig. 3i compares the contact angles of each  
 6 solvent on the bare and OTS-treated PDL surfaces, showing a marked increase in  
 7 hydrophobicity after the OTS treatment for all solvents. Evidently, this improved  
 8 hydrophobicity contributed to enhanced ink confinement within the pixel cavities. As shown  
 9 in Fig. 3i, the contact angle of the OTS-treated PDL was measured to be 106°, confirming  
 10 successful hydrophobic surface modification. In all solvents, the OTS treatment increased the  
 11 contact angle, thereby enhancing the hydrophobicity and improving ink confinement within  
 12 the pixel cavities.



13  
 14 **Fig. 3.** Optical microscope images of assembled fin-LEDs using different solvents: **a** acetone, **b** GBL,  
 15 **c** ethylene glycol, and **d** polyethylene glycol. SEM images of fin-LEDs assembled using different  
 16 solvents: **e** acetone, **f** GBL, **g** ethylene glycol, and **h** polyethylene glycol. **i** Contact angles and images  
 17 (inset) of bare PDL and OTS-treated PDL for each solvent. **j** Average number of fin-LEDs per pixel  
 18 assembled using each solvent-based fin-LED ink. **k** Assembly ratio of fin-LEDs using various ink

1 solvents.

2 To address this limitation, a bi-solvent system combining acetone and PEG was  
3 introduced. The aim of this approach was to maintain effective solvent trapping while  
4 enhancing both the p-GaN contact ratio and the number of assembled fin-LEDs within each  
5 pixel (Fig. 4). As shown in Fig. 4, PEG and acetone were mixed at three different volume ratios:  
6 25, 50, and 75 vol%. The optical images of the assembled fin-LEDs presented in Figs. 4a–c  
7 reveal that the number of assembled LEDs within each pixel gradually decreased with  
8 increasing PEG concentration. This is attributed to the higher viscosity of PEG, which limited  
9 the mobility of the fin-LEDs under DEP. The results of the quantitative analysis presented in  
10 Fig. 4e show that the average number of fin-LEDs per pixel was highest at 25 vol% PEG, with  
11 an average of 9.6 devices and a relatively low standard deviation. As the PEG content increased  
12 to 50 and 75 vol%, the average decreased significantly, indicating insufficient DEP-induced  
13 assembly. Additionally, as shown in Fig. 4d, the assembly ratio reached 100% at 25 vol% PEG,  
14 confirming that solvent trapping was effective under these conditions. The uniform yield also  
15 reached its highest value of 57.3%, suggesting that the pixel-level consistency was improved.  
16 Importantly, the overlap between the fin-LEDs was significantly reduced when the PEG–  
17 acetone mixture was used. As shown in Fig. 4f, the percentage of overlapping fin-LEDs  
18 decreased to 10% at 25 vol% PEG, whereas 90% of the devices exhibited an accurate, non-  
19 overlapping assembly. This represents a major improvement compared to the overlap ratio  
20 observed under the single-solvent conditions depicted in Fig. 3. Overall, the 25 vol% PEG and  
21 acetone mixture provided a favourable balance between fluidic confinement and fin-LED  
22 mobility, which enabled a high assembly ratio, uniform distribution, and minimal overlap  
23 within the pixel array.

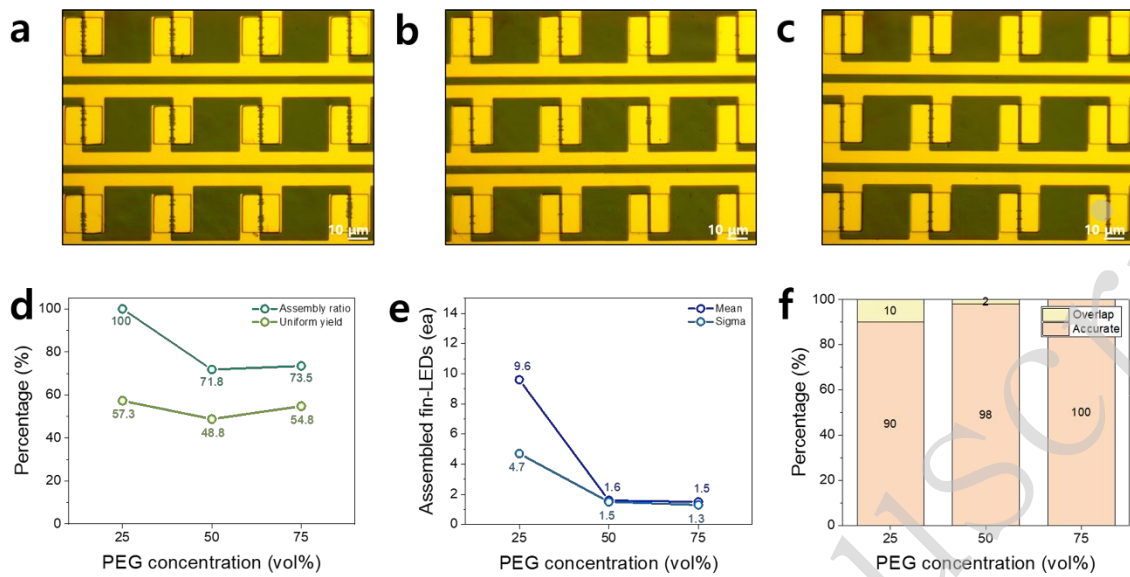
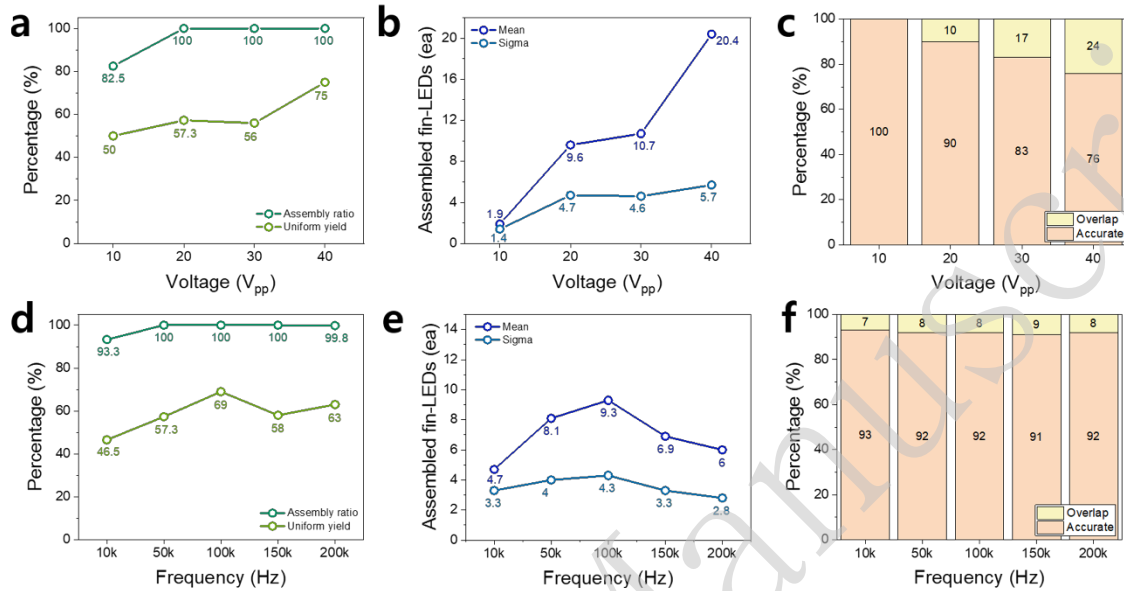


**Fig. 4.** Optical microscope images of assembled fin-LEDs using PEG/acetone mixed solvents with different PEG concentrations: **a** 25 vol%, **b** 50 vol%, and **c** 75 vol%. **d** Assembly ratio and uniform yield as a function of PEG concentration. **e** Mean and standard deviation (sigma) of the number of assembled fin-LEDs per pixel. **f** Ratio of overlapped fins and accurately assembled fin-LEDs for each PEG concentration.

Based on the optimised PEG:acetone = 25:75 (vol%) bi-solvent system, the assembly behaviour was investigated as a function of the applied voltage and frequency, as shown in Fig. 5. As shown in Fig. 5a, when the voltage was increased from 10  $V_{pp}$  to 40  $V_{pp}$  at a fixed frequency of 50 kHz, the assembly ratio improved from 82.5% to 100%, and the uniform assembly yield increased from 50% to a maximum of 75%. In addition, as shown in Fig. 5b, the average number of assembled fin-LEDs per pixel increased significantly from 1.3 at 10  $V_{pp}$  to 20.4 at 40  $V_{pp}$ . However, as shown in Fig. 5c, the number of overlapping fin-LEDs increased with increasing voltage. This indicates that excessive assembly at high voltages leads to overlap. Therefore, 20  $V_{pp}$  was selected as the optimal condition because it yielded a sufficient number of assembled fin-LEDs per pixel with a low overlap rate. Based on this, the assembly characteristics were further analysed by varying the frequency from 10 to 200 kHz. As shown in Fig. 5d, the assembly ratio remained relatively stable, with values greater than 93% under all conditions. As evident from Fig. 5e, the average number of assembled fin-LEDs per pixel peaked at 9.3 at 100 kHz, while relatively fewer fin-LEDs were assembled at other frequencies. Fig. 5f shows that the overlap rate remained low (8%–9%) across most frequency conditions, whereas the accurate assembly rate was consistently above 90%. These results indicate that the

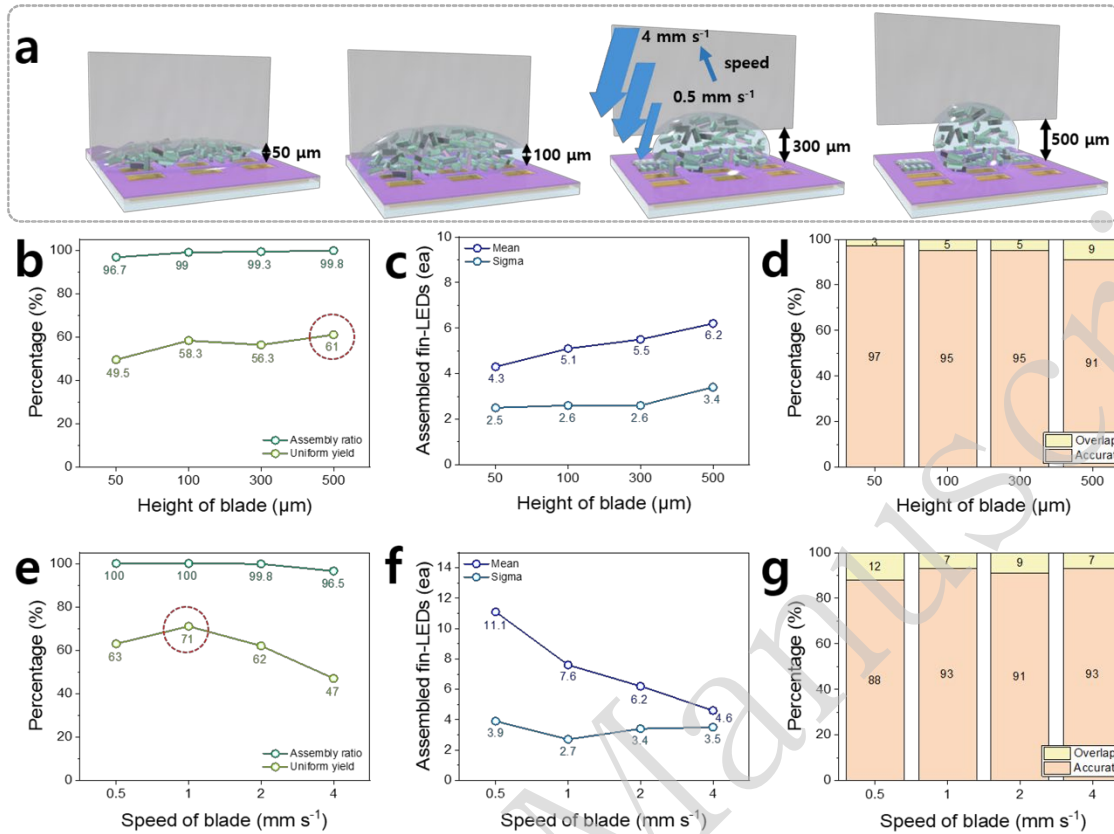
1 frequency does not significantly affect assembly uniformity or accuracy. Therefore, 100 kHz  
 2 and 20  $V_{pp}$  were identified as the optimal conditions to achieve a trapped assembly.



3  
 4 **Fig. 5.** a Assembly ratio and uniform yield as a function of applied voltage. b Mean and standard  
 5 deviation (sigma) of the number of assembled fin-LEDs per pixel at different voltages. c Ratio of  
 6 overlapped fin-LEDs and accurately assembled fins for each voltage condition. d Assembly ratio and  
 7 uniform yield as a function of applied frequency. e Mean and standard deviation (sigma) of the number  
 8 of assembled fin-LEDs per pixel at different frequencies. f Ratio of overlapped fins and accurately  
 9 assembled fin-LEDs for each frequency condition with optical microscope images (inset).

10 Fig. 6a presents the effect of blade height and blade moving speed on the assembly  
 11 behaviour of fin-LEDs under the conditions of a PEG:acetone = 25:75 (vol%) mixed solvent  
 12 with an electrical input of 20  $V_{pp}$  and 100 kHz. To investigate the effect of blade height, the  
 13 distance was varied from 50 to 500  $\mu\text{m}$ . As can be observed in Fig. 6b, the assembly ratio  
 14 increased from 96.7% to 99.8% with increasing blade height, whereas the uniform assembly  
 15 yield improved from 49.5% to 61%. This trend can be attributed to a reduction in the physical  
 16 pressure applied by the blade on the droplet, which limited spreading and provided a more  
 17 stable DEP-based assembly. Fig. 6c shows that the average number of fin-LEDs assembled per  
 18 pixel also increased with blade height, reaching a maximum of 6.2 at 500  $\mu\text{m}$ . However, as  
 19 seen in Fig. 6d, the overlap rate also rose with increasing height, with a 9% overlap observed  
 20 at 500  $\mu\text{m}$ , indicating a corresponding decrease in accurate assembly. Next, the effect of blade  
 21 speed was examined under conditions ranging from 0.05 to 4  $\text{mm s}^{-1}$ . As shown in Fig. 6e, the

1 highest uniform assembly yield of 71% was obtained at a speed of  $1 \text{ mm s}^{-1}$ . At  $0.5 \text{ mm s}^{-1}$ , the  
2 yield was 63%, while at  $4 \text{ mm s}^{-1}$  it dropped to 47%, which indicated that assembly uniformity  
3 clearly depended on blade speed. In Fig. 6f, an average of 11.1 fin-LEDs were assembled per  
4 pixel at  $0.05 \text{ mm s}^{-1}$ , but the number decreased as the speed increased. This is likely due to the  
5 longer DEP exposure time at lower speeds, which allows more fin-LEDs to be attracted.  
6 However, as shown in Fig. 6g, the overlap rate was the highest at 12% under  $0.05 \text{ mm s}^{-1}$ . This  
7 suggests an excessive assembly of LED due to overlap-related defects. In contrast, the overlap  
8 rate at  $1 \text{ mm s}^{-1}$  was lower at 7 while the accurate assembly rate was maintained at 93%, and  
9 accordingly, this was determined to be the optimal blade speed. Therefore, a blade height of  
10  $500 \text{ }\mu\text{m}$  and a blade speed of  $1 \text{ mm s}^{-1}$  were identified as the critical operating conditions that  
11 simultaneously maximise assembly ratio and uniform yield while ensuring overall process  
12 stability and reproducibility. These findings demonstrate that both the blade height and blade  
13 speed are decisive parameters that directly influence the number of assembled fin-LEDs,  
14 assembly uniformity, and overlap rate. Consequently, the precise optimisation of each  
15 parameter is essential for achieving high-performance DEP-based assemblies. Based on the  
16 optimised assembly conditions described above, the effect of the dispersion concentration was  
17 evaluated by separating the fin-LEDs from a quarter section of a 4-inch GaN-on-sapphire wafer  
18 and dispersing them in 6 mL of the optimised 25 vol% PEG solvent to prepare a stock solution.  
19 Based on this stock solution, inks with three different relative concentrations ( $\times 1$ ,  $\times 2$ , and  $\times 3$ )  
20 were prepared, quantified using UV-Vis spectroscopy, and subsequently used to examine the  
21 assembly performance. The assembly results shown in Fig. S5 revealed that higher  
22 concentrations led to an increased uniform yield; however, the average number of assembled  
23 fin-LEDs per pixel also increased to 13.7, resulting in a higher overlap ratio. Conversely, lower  
24 concentrations reduced the overlap but decreased both the uniform yield and the number of  
25 assembled fin-LEDs. Considering these trade-offs, we determined that the  $\times 2$  concentration  
26 provided the best balance between assembly consistency and minimal overlap and therefore  
27 used this concentration as the optimal condition for subsequent experiments.



1  
2 **Fig. 6.** **a** Schematic of the height of blade and speed of blade during assembly process. **b**  
3 Assembly ratio and uniform yield as a function of blade height. **c** Mean and standard deviation  
4 (sigma) of the number of assembled fin-LEDs per pixel at different blade heights. **d** Ratio of  
5 overlapped fins and accurately assembled fin-LEDs for each blade height condition. **e**  
6 Assembly ratio and uniform yield as a function of blade speed. **f** Mean and standard deviation  
7 (sigma) of the number of assembled fin-LEDs per pixel at different blade speeds. **g** Ratio of  
8 overlapped fin-LEDs and accurately assembled fins for each blade speed condition.

9 Fig. 7 illustrates the effect of blade coating repetition on the assembly characteristics of  
10 fin-LEDs under identical DEP assembly conditions (PEG:acetone = 25:75 vol%, 20  $V_{pp}$ , 50  
11 kHz) using a blade speed of 1  $\text{mm s}^{-1}$  and a blade height of 500  $\mu\text{m}$ . As the number of blades  
12 passing over the same position increased, the probability of guiding the fin-LEDs toward the  
13 electrode was expected to improve because of the repeated exposure to the electric field. To  
14 evaluate this, single-, double-, and triple-pass blade coatings were applied and compared, as  
15 shown in the optical microscopy images in Figs. 7a–c. As shown in Fig. 7d, the uniform  
16 assembly yield increased progressively with the number of blade passes: 57.8% for a single-  
17 pass, 67.3% for a double-pass, and 84.8% for a triple-pass. The overall assembly ratio remained

1 above 99% across all conditions, with the triple-pass method achieving 100% assembly. These  
2 results suggest that repeated blade coating enhances the number of assembled pixels and  
3 improves assembly uniformity. As shown in Fig. 7e, the average number of assembled fin-  
4 LEDs per pixel also increased with additional passes—from 8.1 for the single-pass to 12.7 for  
5 the double-pass and 16.7 for the triple-pass. Meanwhile, the standard deviation remained below  
6 four in all cases, indicating consistent assembly results. Fig. 7f shows that the overlap ratio  
7 increased slightly with more blade passes, measuring 10% for both the single-pass and double-  
8 pass and 12% for the triple-pass. Nevertheless, the assembly ratio remained above 88% under  
9 all conditions (Fig. 7g). This suggests that, while repeated passes improve the assembly  
10 quantity and uniformity, they may introduce a slight increase in overlap owing to over-  
11 assembly. Overall, increasing the number of blade passes is an effective approach for  
12 enhancing the assembly efficiency and uniformity of fin-LEDs. Among the tested conditions,  
13 the triple-pass blade coating provided the highest assembly yield and uniformity while  
14 maintaining a high degree of accuracy; thus, it was the optimal process condition. In addition,  
15 when the electroluminescent (EL) devices were fabricated under each blade-pass condition, the  
16 triple-pass process resulted in more uniform emission across the pixels compared to the single-  
17 pass process, as shown in Fig. 7c. This is attributed to the higher number of assembled fin-  
18 LEDs per pixel in the triple-pass condition, as also seen when contrasted with Fig. 7a.

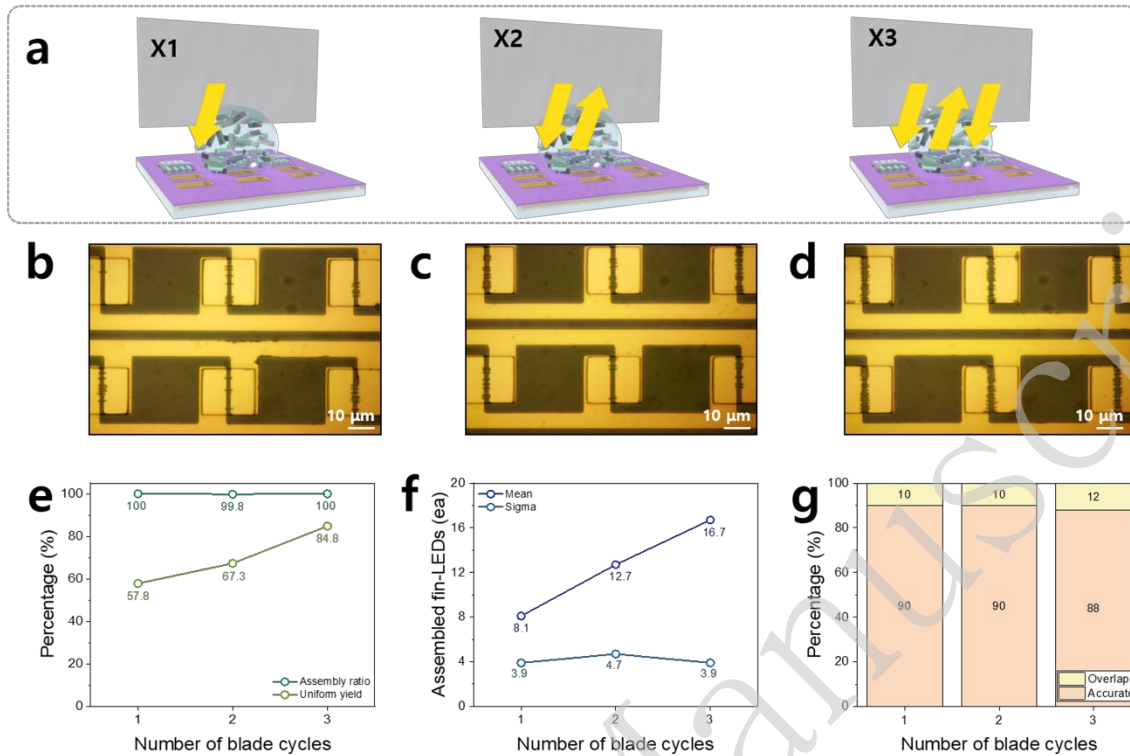
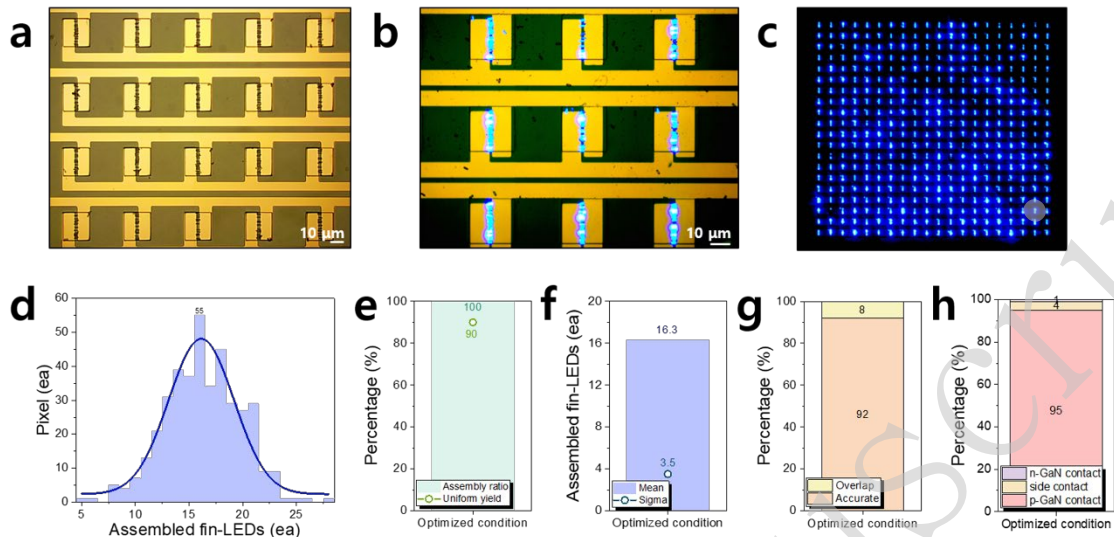


**Fig. 7.** **a** Schematic of the number of blade cycles during the assembly process. Optical microscope images after **b** one cycle, **c** two cycles, and **d** three cycles. **e** Assembly ratio and uniform yield as a function of the number of blade cycles. **f** Mean and standard deviation (sigma) of the number of assembled fin-LEDs per pixel for different blade cycles. **g** Ratio of overlapped fins and accurately assembled fin-LEDs for each blade cycle condition.

Fig. 8 presents the comprehensive results of the fin-LED assembly achieved under the optimised process conditions. In this study, a mixed solvent of PEG and acetone at a ratio of 25:75 (vol%) was used, and the electric field conditions were set to 100 kHz and 20  $V_{pp}$ . The blade coating process was carried out at a speed of 1 mm  $s^{-1}$ , with a blade height of 500  $\mu m$  and triple-pass coating. These conditions were selected as the optimal conditions based on previous parametric experiments in which the highest assembly uniformity and accuracy were demonstrated. Fig. 8a shows an optical microscopy image of the entire array assembled under the optimised conditions, confirming that the fin-LEDs were successfully assembled in all pixels. The assembled fin-LEDs were then used to fabricate EL devices. Fig. 8b shows a magnified image of a single pixel, clearly showing the fin-LEDs trapped and assembled within the electrodes. Fig. 8c presents an EL image of the assembled array, wherein most of the pixels exhibit uniform emission, indicating excellent assembly uniformity and reliable electrical contact.

1 Fig. 8d shows a histogram of the number of assembled fin-LEDs per pixel. Out o  
2 f 400 pixels, 360 exhibited fin-LED counts within the range of 12–20, corresponding  
3 to a uniform assembly yield of 90%. Fig. 8e shows an overall assembly ratio of 100%  
4 and uniform assembly yield of 90%. Fig. 8f shows that the average number of asse  
5 mbled fin-LEDs per pixel was 16.3, with a standard deviation of 3.5, demonstrating a  
6 consistent assembly performance. As shown in Fig. 8g, the overlap ratio was 8%, an  
7 d the accurate assembly ratio reached 92%, indicating that a high assembly density w  
8 as maintained without significant overlap. Finally, Fig. 8h shows that 95% of the asse  
9 mbled fin-LEDs were in contact with the p-GaN surface. This confirms that the solve  
10 nt composition plays a critical role in determining the assembly orientation. These res  
11 ults demonstrate that precise control of the solvent composition, electric field conditio  
12 ns, and blade parameters enables the implementation of a highly accurate and uniform  
13 DEP-based assembly process for fin-LEDs. To accurately evaluate the emission charac  
14 teristics of the fin-LEDs, we first fabricated a test cell with an active area of  $1\text{ mm} \times 1$   
15  $\text{mm}$ , an electrode width of  $10\text{ }\mu\text{m}$ , and an electrode spacing of  $2\text{ }\mu\text{m}$ , as shown in Fig.  
16 S6. This test structure was designed to reliably probe the intrinsic emission behaviour of  
17 fin LEDs, which cannot be directly assessed in a highly integrated array geometry. The  
18 EL measurements from the test cell exhibited a maximum EQE of approximately 8.2% a  
19 t a current density of  $0.011\text{ A cm}^{-2}$  and a luminance of  $6121\text{ cd m}^{-2}$  at  $0.25\text{ A cm}^{-2}$ , con  
20 firming the high performance of the individual fin-LED emitters. The EL characteristics  
21 of the array cell fabricated under the optimised conditions were also evaluated. The arra  
22 y cell exhibited a maximum EQE of 3.26% at a current density of  $0.0157\text{ A cm}^{-2}$  and a  
23 luminance of  $1584\text{ cd m}^{-2}$  at  $0.28\text{ A cm}^{-2}$  (Fig. S6). Evidently, the lower luminance obse  
24 rved in the array cell compared to the test cell is attributable to the relatively large pixel  
25 pitch of  $70\text{ }\mu\text{m}$ , which increases the ratio of non-emissive to emissive areas and thereby  
26 limits the effective emission area and light-extraction efficiency. In addition, consistent  
27 EL characteristics were obtained for multiple test cells fabricated using the same DEP-ba  
28 sed alignment and assembly process, demonstrating the high reproducibility of the optimi  
29 sed process and its applicability to various device configurations. These results indicate t  
30 hat further optimisation of the device structure and fabrication process can enhance the p  
31 erformance of the array configuration, suggesting a strong potential for future high-resolu  
32 tion display applications.



1  
2 **Fig. 8.** **a** Optical microscope image and **b** high-magnification optical microscope image showing the  
3 fin-LED assembly under the optimized conditions: 25 vol% PEG, 20  $V_{pp}$ , 100 kHz, blade speed of 1  
4 mm s<sup>-1</sup>, blade height of 500  $\mu$ m, and three cycles. **c** EL image of the fin-LED device under the optimized  
5 conditions. **d** Distribution of fin-LED counts per pixel. **e** Assembly ratio and uniform yield. **f** Mean and  
6 standard deviation (sigma) of the number of assembled fin-LEDs per pixel. **g** Ratio of overlapped fins  
7 and accurately assembled fin-LEDs under the optimized conditions.

## 8 Discussion

9 In this study, we propose a high-precision assembly technique to implement high-resolution nano-  
10 to microscale displays based on a trapped-assembly method that combines a doctor-blade-based ink-  
11 delivery system with DEP-induced assembly. This method effectively confines the ink within  
12 individual pixels to minimise the diffusion and aggregation of fin-LEDs during the assembly process  
13 and enhances the overall stability. To this end, OTS SAMs were applied to the PDL to induce ink  
14 trapping and establish trapped-assembly conditions. The key process parameters, including the  
15 viscosity and dielectric properties of the ink solvent, speed and number of blade passes, gap between  
16 the blade and the substrate, and applied DEP voltage and frequency, were systematically optimised.  
17 The optimal conditions were thereupon identified as a PEG:acetone bi-solvent at 25:75 vol%, a DEP  
18 voltage of 20  $V_{pp}$ , a frequency of 100 kHz, a blade height of 500  $\mu$ m, a blade speed of 1 mm s<sup>-1</sup>, and  
19 triple-pass coating. Under these conditions, successful fin-LED assembly was achieved for all 400  
20 pixels, with 90% of the pixels containing 12–20 fin-LEDs per pixel. The average number of assembled  
21 fin-LEDs was 16.3 with a standard deviation of 3.5. The overlap ratio was 8%, and 92% of the fin-  
22 LEDs were accurately assembled. In addition, 95% of the fin-LEDs were in contact with the p-GaN

1 surface, indicating effective orientation control. The EL devices fabricated using the assembled fin-  
2 LEDs exhibited bright and uniform emissions across the entire pixel array, which confirmed not only  
3 the excellent assembly quality but also the high electrical reliability.

4 In conclusion, the DEP-based trapped-assembly method developed in this study provides a reliable  
5 and scalable process strategy for achieving a high-yield, high-accuracy pixel-level assembly of fin-  
6 LEDs. By effectively overcoming the limitations of conventional fluidic assembly techniques, this  
7 approach demonstrates clear potential for extension to large-area and flexible substrates and further  
8 shows applicability to display systems employing colour-conversion layers. Therefore, the proposed  
9 method is expected to serve as a promising solution for practical integration of nanoscale and microscale  
10 LEDs into next-generation high-resolution display technologies.

## 12 **Materials and Methods**

### 13 **Fabrication of fin-LEDs**

14 The blue epitaxial wafer used in this study was purchased from SEMITEK Co. (Taiwan) and  
15 consisted of a 50 nm p-GaN layer, a 150 nm InGaN/GaN multiple quantum well (MQW) structure,  
16 and a 2.0  $\mu\text{m}$  n-GaN layer, and a 1.5  $\mu\text{m}$  u-GaN layer. To form the current-spreading layer, a  
17 150 nm indium tin oxide (ITO) film was deposited using RF sputtering. Subsequently, a  
18 bilayer hard mask consisting of 200 nm aluminium and 900 nm SiO<sub>2</sub> layers was sequentially  
19 deposited using an electron beam evaporator and plasma-enhanced chemical vapour  
20 deposition (PECVD), respectively. Nanoimprint lithography was used to define the fin-LED  
21 structures. For this process, a spin-on-glass (SOG) material (FOX-16, DOW Corning Co.)  
22 was spin-coated onto a PDMS mould (Sylgard® 184, Dow Corning Co.), which was then  
23 laminated onto the masked GaN wafer under uniform pressure to transfer the fin-like  
24 nanopattern onto the Al layer. The hard mask was etched by sequentially removing the Al and  
25 SiO<sub>2</sub> layers using chlorine-based inductively coupled plasma (ICP) and fluorine-based  
26 reactive-ion etching (RIE), respectively. The patterned GaN structure was subsequently  
27 etched using Cl<sub>2</sub>-based ICP to define the fin-LED structures.

28 To mitigate plasma-induced damage during dry etching, the sample was treated with  
29 tetramethylammonium hydroxide (TMAH, 25 wt% in water, Sigma-Aldrich) at 80 °C for five  
30 minutes. To suppress excessive porosity during subsequent electrochemical etching (ECE), a

1 50 nm-thick SiO<sub>2</sub> layer was deposited via PECVD. After partial removal of the n-GaN bottom  
2 region, the ECE process was carried out in a 0.3 M oxalic acid solution for 5 min to induce  
3 porosity and enable detachment of the fin-LEDs from the substrate. Following the ECE  
4 process, the SiO<sub>2</sub> protective layer was eliminated using a buffer oxide etchant (BOE), and a  
5 passivation layer was applied. The detached fin-LEDs were released from the wafer after 5  
6 min of sonication in gamma-butyrolactone (GBL), followed by solvent exchange and  
7 purification using acetone.

### 8 **Trapped-assembly of fin-LEDs**

9 As shown in Fig. S7, the first step of the fin-LED assembly process involved the patterning  
10 of the electrodes using a photolithography process with a negative photoresist to achieve  
11 precise assembly and placement within each pixel. Subsequently, 10 nm of Cr and 200 nm of  
12 Au layers were deposited using an e-beam evaporator. A lift-off process with acetone was  
13 then performed to form electrode pairs with a width of 15 μm and a gap of 2 μm. To  
14 concentrate the electric field within each pixel, a PDL was formed on top of the electrodes  
15 using SU8 2002 photoresist and then patterned into 400 square pixels with dimensions of 30  
16 μm × 30 μm and a pitch of 70 μm.

17 To implement the trapped-assembly method, a self-assembled monolayer (SAM) of OTS  
18 was selectively formed on the surface of SU8-based PDL to induce hydrophobicity. A positive  
19 photoresist (AZ 5214) was first coated and then selectively exposed to the same mask, leaving  
20 only the PR inside the pixel regions. After the O<sub>2</sub> plasma treatment, hydroxyl groups were  
21 introduced on the SU8 surface. The substrate was then immersed in a solution of 10 μL of  
22 OTS in 20 mL of anhydrous hexane for 1 h to form SAMs. Finally, the PR inside the pixel  
23 was removed using acetone, resulting in a selective OTS coating on the SU8 PDL.

24 The assembly process was conducted using the trapped-assembly approach. A 3 μL droplet  
25 of fin-LED ink dispersion was placed outside the active electrode area and then dragged  
26 across the pixelated region using a doctor blade. The ink was effectively confined within the  
27 pixel cavities, while the fin-LEDs were directed and assembled into the pixels under the  
28 influence of DEP. This process relied on three cooperative mechanisms: surface energy  
29 control achieved through the OTS treatment, physical trapping driven by blade motion, and  
30 electrical assembly induced by DEP, all of which contribute to the achievement of a highly  
31 oriented and precise assembly. To further investigate the assembly characteristics, various

1 parameters, including ink-solvent properties, DEP voltage and frequency, blade speed and  
2 stroke count, and vertical gap between the blade and electrodes, were systematically varied  
3 and analysed.

4 A quantitative evaluation was performed by analysing all 400 pixels based on three metrics:  
5 the assembly ratio, uniform yield, and overlapped fin-LED yield. Pixels containing at least  
6 one fin-LED were considered active and used to calculate the assembly ratio. Pixels with a  
7 number of fin-LEDs within  $\pm 30\%$  of the average were categorised as uniform, and the  
8 corresponding uniform yield was determined. Additionally, the number of pixels containing  
9 overlapping fin-LEDs was counted to calculate the yield of the overlapped fin-LEDs and  
10 comprehensively assess the overall assembly quality.

### 11 **Fabrication of the fin-LED EL device**

12 Electroluminescent devices were fabricated using fin-LEDs assembled within 400 pixels.  
13 First, a 40 nm SiO<sub>2</sub> layer was deposited via electron-beam evaporation to provide mechanical  
14 anchoring. An insulating layer was then formed using SU-8 photoresist, exposing the p-pad  
15 electrodes. Dry etching was performed using RIE to expose the n-GaN faces of the fin-LEDs.  
16 Finally, a 500 nm transparent conductive oxide layer composed of aluminium-doped zinc  
17 oxide (AZO) was deposited across the entire surface via RF sputtering to complete the device  
18 fabrication.

### 19 **Characterization**

20 The structural characteristics of the fabricated fin-LEDs were examined using scanning  
21 electron microscopy (SEM, JSM-7610F; JEOL Ltd., Japan). X-ray diffraction (XRD, Ultima  
22 IV, Rigaku) and Raman spectroscopy ( $\lambda = 532$  nm, Nd:YAG laser) were used to evaluate the  
23 crystallinity and overall structural integrity of the fin LED array. Transmission electron  
24 microscopy (TEM, JEM-2100F, JEOL Ltd., 200 kV) was used to analyse the microstructures  
25 of the individual fin-LEDs. The quality of the fin-LED assembly was quantitatively assessed  
26 by a statistical analysis of the optical and SEM imaging data. To characterise optical  
27 properties, photoluminescence (PL) was measured using a Ti:Sapphire laser ( $\lambda = 355$  nm).  
28 The electroluminescence (EL) behaviour and current–voltage–luminance (IVL) responses of  
29 the fabricated devices were recorded using a CS-2000 spectroradiometer (Konica Minolta)  
30 and a Keithley 2001 source meter (Keithley Instruments Inc.).

1

## 2 **Acknowledgements**

3 † M. K. and Y.K. contributed equally to this work.

4 This work was supported by a National Research Foundation of Korea (NRF) grant funded by  
5 the Korea government (MSIT) (RS-2021-NR059326) and the Nano & Material Technology  
6 Development Program through the National Research Foundation of Korea (NRF) funded by  
7 Ministry of Science and ICT(RS-2023-00281346).

8

## 9 **Author Contributions**

10 Y.R. Do supervised the whole project. Y. Kwon and M. Ko conceived the experiments. S. Lee  
11 and H. Oh carried out the experiments. K.N. Lee characterized the data. M. Ko drafted the  
12 manuscript. All the authors discussed the results and contributed to the final version of the  
13 manuscript

## 14 **Data availability**

15 All data are available from the corresponding authors upon reasonable request.

16

## 17 **Conflict of interest**

18 The authors declare no competing interests.

19

## 20 **Supplementary information**

21 Supplementary materials are available at the online version.

22

## 23 **References**

24 1. Wu, T. Z. et al. Mini-LED and micro-LED: promising candidates for the next  
25 generation display technology. *Applied Sciences* **8**, 1557 (2018) doi:  
26 10.3390/app8091557

27 2. Huang, Y. G. et al. Prospects and challenges of mini-LED and micro-LED

- 1 displays. *Journal of the Society for Information Display* **27**, 387-401 (2019) doi:  
2 10.1002/jsid.760.
- 3 3. Huang, Y. G. et al. Mini-LED, Micro-LED and OLED displays: present status  
4 and future perspectives. *Light: Science & Applications* **9**, 105 (2020) doi:  
5 10.1038/s41377-020-0341-9.
- 6 4. Hsiang, E. L. et al. Prospects and challenges of mini-LED, OLED, and micro-  
7 LED displays. *Journal of the Society for Information Display* **29**, 446-465 (2021) doi:  
8 10.1002/jsid.1058.
- 9 5. Anwar, A. R. et al. Recent progress in micro-LED-based display technologies.  
10 *Laser & Photonics Reviews* **16**, 2100427 (2022) doi: 10.1002/lpor.202100427.
- 11 6. Lin, C. C. et al. The micro-LED roadmap: status quo and prospects. *Journal*  
12 *of Physics: Photonics* **5**, 042502 (2023) doi: 10.1088/2515-7647/acf972.
- 13 7. Ma, T. et al. Progress in color conversion technology for Micro-LED.  
14 *Advanced Materials Technologies* **8**, 2200632 (2023) doi: 10.1002/admt.202200632.
- 15 8. Do, Y. R. & Yoo, G. Y. MicroLEDs get in line. *Nature Electronics* **6**, 182-183  
16 (2023) doi: 10.1038/s41928-023-00937-9.
- 17 9. Kim, T. S. et al. Future trends of display technology: micro-LEDs toward  
18 transparent, free-form, and near-eye displays. *Light: Science & Applications* **14**, 335  
19 (2025) doi: 10.1038/s41377-025-02027-1.
- 20 10. Jin, H. J. et al. Micro-LED retinal projection for augmented reality near-eye  
21 displays. *Laser & Photonics Reviews* **19**, 2402083 (2025) doi:  
22 10.1002/lpor.202402083.
- 23 11. Chen, G. J. et al. Microfluidics implemented high stability tunable structural  
24 color device for display and optical encryption. *Plasmonics* **20**, 7619-7629 (2025) doi:  
25 10.1007/s11468-025-02797-9.
- 26 12. Chen, Z., Yan, S. K. & Danesh, C. MicroLED technologies and applications:  
27 characteristics, fabrication, progress, and challenges. *Journal of Physics D: Applied*  
28 *Physics* **54**, 123001 (2021) doi: 10.1088/1361-6463/abcfe4.

- 1 13. Liu, Z. J. et al. Micro-light-emitting diodes with quantum dots in display  
2 technology. *Light: Science & Applications* **9**, 83 (2020) doi: 10.1038/s41377-020-  
3 0268-1.
- 4 14. Chen, D. B. et al. Integration technology of micro-LED for next-generation  
5 display. *Research* **6**, 0047 (2023) doi: 10.34133/research.0047.
- 6 15. Chen, E. G. et al. Broadband beam collimation metasurface for full-color  
7 micro-LED displays. *Optics Express* **32**, 10252-10264 (2024) doi:  
8 10.1364/OE.518535.
- 9 16. Ryu, J. E. et al. Technological breakthroughs in chip fabrication, transfer, and  
10 color conversion for high-performance micro-LED displays. *Advanced Materials* **35**,  
11 2204947 (2023) doi: 10.1002/adma.202204947.
- 12 17. Miao, W. C. et al. Microdisplays: mini-LED, micro-OLED, and micro-LED.  
13 *Advanced Optical Materials* **12**, 2300112 (2024) doi: 10.1002/adom.202300112.
- 14 18. Lee, T. Y. et al. Technology and applications of micro-LEDs: their  
15 characteristics, fabrication, advancement, and challenges. *ACS Photonics* **9**, 2905-  
16 2930 (2022) doi: 10.1021/acsp Photonics.2c00285.
- 17 19. Tian, P. et al. Micro-LED based optical wireless communications systems.  
18 *Semiconductors and Semimetals* **106**, 281-321 (2021) doi:  
19 10.1016/bs.semsem.2021.01.003.
- 20 20. Lee, V. W., Twu, N. & Kymissis, I. Micro-LED technologies and applications.  
21 *Information Display* **32**, 16-23 (2016) doi: 10.1002/j.2637-496X.2016.tb00949.x.
- 22 21. Zhu, G. Q. et al. Mass transfer, detection and repair technologies in micro-  
23 LED displays. *Science China Materials* **65**, 2128-2153 (2022) doi: 10.1007/s40843-  
24 022-2110-2.
- 25 22. Li, J. Y. et al. Study of transfer-printing technologies for micro-LED displays.  
26 *SID China Spring Online Technical Meeting Proceedings* **51**, 125-128 (2020) doi:  
27 10.1002/sdtp.13769.
- 28 23. Park, S. I. et al. Printed assemblies of inorganic light-emitting diodes for

- 1 deformable and semitransparent displays. *Science* **325**, 977-981 (2009) doi:  
2 10.1126/science.1175690.
- 3 24. Kim, S. et al. Microstructured elastomeric surfaces with reversible adhesion  
4 and examples of their use in deterministic assembly by transfer printing. *Proceedings*  
5 *of the National Academy of Sciences of the United States of America* **107**, 17095-  
6 17100 (2010) doi: 10.1073/pnas.1005828107.
- 7 25. Yoon, S. U. et al. Transfer of micro-LEDs with roll-based direct overlay  
8 alignment for manufacturing transparent displays. *Advanced Electronic Materials* **10**,  
9 2400236 (2024) doi: 10.1002/aelm.202400236.
- 10 26. Meitl, M. et al. 55-1: *Invited paper*: passive matrix displays with transfer-printed  
11 microscale inorganic LEDs. *SID Symposium Digest of Technical Papers* **47**, 743-746 (2016)  
12 doi: 10.1002/sdtp.10748.
- 13 27. Saeidpourazar, R. et al. A prototype printer for laser driven micro-transfer  
14 printing. *Journal of Manufacturing Processes* **14**, 416-424 (2012) doi:  
15 10.1016/j.jmapro.2012.09.014.
- 16 28. Luo, H. Y. et al. Laser-driven transfer printing techniques for micro-LED  
17 display. in *Transfer Printing Technologies and Applications* (eds Cao, C. H. & Sun,  
18 Y.) (Amsterdam: Elsevier, 2024), 325-351. doi: 10.1016/B978-0-443-18845-  
19 9.00013-2.
- 20 29. Sun, W. G. et al. 20  $\mu\text{m}$  micro-LEDs mass transfer via laser-induced in situ  
21 nanoparticles resonance enhancement. *Small* **20**, 2309877 (2024) doi:  
22 10.1002/smll.202309877.
- 23 30. Cui, Y. X. et al. Application of laser-assisted bonding in micro-LED display  
24 technology. *Journal of the Society for Information Display* **33**, 873-879 (2025) doi:  
25 10.1002/jsid.2057.
- 26 31. Marinov, V. R. 52-4: Laser-enabled extremely-high rate technology for  $\mu\text{LED}$   
27 assembly. *SID Symposium Digest of Technical Papers* **49**, 692-695 (2018) doi:  
28 10.1002/sdtp.12352.
- 29 32. Cho, S., Lee, D. & Kwon, S. Fluidic self-assembly transfer technology for

- 1 micro-LED display. 2019 20th International Conference on Solid-State Sensors,  
2 Actuators and Microsystems & Eurosensors XXXIII (TRANSDUCERS &  
3 EUROSENSORS XXXIII). Berlin, Germany: IEEE, 2019. 402-404. doi:  
4 10.1109/TRANSDUCERS.2019.8808352.
- 5 33. Hwang, J. et al. Wafer-scale alignment and integration of micro-light-emitting  
6 diodes using engineered van der Waals forces. *Nature Electronics* **6**, 216-224 (2023)  
7 doi: 10.1038/s41928-022-00912-w.
- 8 34. Lee, D. et al. Fluidic self-assembly for MicroLED displays by controlled  
9 viscosity. *Nature* **619**, 755-760 (2023) doi: 10.1038/s41586-023-06167-5.
- 10 35. Chang, W. et al. Concurrent self-assembly of RGB microLEDs for next-  
11 generation displays. *Nature* **617**, 287-291 (2023) doi: 10.1038/s41586-023-05889-w.
- 12 36. Sheen, M. et al. Highly efficient blue InGaN nanoscale light-emitting diodes.  
13 *Nature* **608**, 56-61 (2022) doi: 10.1038/s41586-022-04933-5.
- 14 37. Cho, H. et al. Efficiency enhancement of submicron-size light-emitting diodes  
15 by triple dielectric layers. *Journal of the Society for Information Display* **31**, 289-297  
16 (2023) doi: 10.1002/jsid.1220.
- 17 38. Kim, T. et al. Enhanced quantum efficiency of horizontally aligned individual  
18 InGaN/GaN nanorod LEDs by self-assembled Ag nanoparticles. *Applied Surface*  
19 *Science* **656**, 159706 (2024) doi: 10.1016/j.apsusc.2024.159706.
- 20 39. Kulkarni, M. A. et al. Monolithic integration of GaN thin film and GaN  
21 nanorods pixels: facile growth of InGaN/GaN quantum wells for the realization of full  
22 color micro-LED display. *Advanced Optical Materials*, **13**, 2500271 (2025) doi:  
23 10.1002/adom.202500271.
- 24 40. Jang, P. K. et al. Integration of InGaN/GaN microrod light emitting diodes on  
25 flexible and peelable substrate via dielectrophoretic alignments. *ACS Photonics* **12**,  
26 513-521 (2025) doi: 10.1021/acsp Photonics.4c02016.
- 27 41. Park, H. K. et al. Horizontally assembled green InGaN nanorod LEDs:  
28 scalable polarized surface emitting LEDs using electric-field assisted assembly.  
29 *Scientific Reports* **6**, 28312 (2016) doi: 10.1038/srep28312.

- 1 42. Eo, Y. J. et al. Enhanced DC-operated electroluminescence of forwardly  
2 aligned p/MQW/n InGaN nanorod LEDs via DC offset-AC dielectrophoresis. *ACS*  
3 *Applied Materials & Interfaces* **9**, 37912-37920 (2017) doi: 10.1021/acsami.7b09794.
- 4 43. Ko, M. et al. Development and isolation of dot LEDs for display applications  
5 through electrochemical etching and sonochemical separation. *Advanced Functional*  
6 *Materials* **34**, 2303727 (2024) doi: 10.1002/adfm.202303727.
- 7 44. Lee, S. et al. Development of fin-LEDs for next-generation inorganic displays  
8 using face-selective dielectrophoretic assembly. *Nature Communications* **15**, 9536  
9 (2024) doi: 10.1038/s41467-024-53965-0.
- 10 45. Ko, M. et al. Enhancing vertical assembly of Dot-LEDs for display application  
11 using metal chelate coordination chemical linkers. *Applied Surface Science* **681**,  
12 161446 (2025) doi: 10.1016/j.apsusc.2024.161446.
- 13 46. Ko, M. et al. Highly vertically assembled dot-LEDs via ethanedithiol chemical  
14 linker and gamma-butyrolactone solvent for display applications. *Chemical*  
15 *Engineering Journal* **511**, 161868 (2025) doi: 10.1016/j.cej.2025.161868.
- 16 47. Yang, X. et al. An overview on the principle of inkjet printing technique and  
17 its application in micro-display for augmented/virtual realities. *Opto-Electronic*  
18 *Advances* **5**, 210123 (2022) doi: 10.29026/oea.2022.210123.
- 19 48. Shah, M. A. et al. Classifications and applications of inkjet printing technology:  
20 a review. *IEEE Access* **9**, 140079-140102 (2021) doi:  
21 10.1109/ACCESS.2021.3119219.